Bandwidth Dependence of the Ranging Error Variance in Dense Multipath

(Invited Paper)

Stefan Hinteregger, Erik Leitinger, Paul Meissner, Josef Kulmer, and Klaus Witrisal
Graz University of Technology, Austria
email: { stefan.hinteregger, erik.leitinger, paul.meissner, kulmer, witrisal } @tugraz.at

***Abstract*—It is well known that the time-of-flight ranging performance is heavy influenced by multipath propagation within a radio environment. This holds in particular in *dense* multipath channels as encountered in indoor scenarios. The signal bandwidth has a tremendous influence on this effect, as it determines whether the time resolution is sufficient to resolve the useful line-of-sight (LOS) signal component from interfering multipath.**

This paper employs a geometry-based stochastic channel model to analyze and characterize the ranging error variance as a function of the bandwidth, covering the narrowband up to the UWB regimes. The Cramér-Rao lower bound (CRLB) is derived for this purpose. It quantifies the impact of bandwidth, SNR, and parameters of the multipath radio channel and can thus be used as an effective and accurate *channel model* (e.g.) for the cross-layer optimization of positioning systems. Experimental data are analyzed to validate our theoretical results.

I. Introduction

Positioning indoors is a challenging task. Existing systems like global navigation satellite systems (e.g GPS, Galileo) fail at indoor positioning due to the limited visibility of the satellites and the limited signal bandwidth. In indoor scenarios a multitude of multipath components (MPC) cause severe fading and pulse distortion of the received signals making the localization challenging.

Performance bounds for the ranging and positioning capabilities of a system allow for fundamental insight into system design considerations or cross-layer optimization. In [1], [2] the Cràmer Rao lower bound has been investigated for radio and radar scenarios providing insight into the influence of system parameters like the signal to noise ratio (SNR) or the bandwidth.

Ultra-wideband (UWB) radio signals are considered to be most promising for indoor positioning because their fine time resolution allows to separate the arriving MPCs into individual components. To investigate performance bounds and capture the information included in the channel, a proper channel model is paramount. In [3] the stochastic IEEE 802.15.4a channel model has been used to derive the Cràmer Rao lower bound and the Ziv-Zakai bound for positioning indoors. By adding geometrically modeled components to the channel model using a so called geometry-based stochastic channel model, the additional information provided by specular multipath components can be quantified [4].

This work was supported by the Austrian Research Promotion Agency (FFG) within the project REFlex (project number: 845630).

Since bandwidth is a scarce resource, minimal usage reduces the costs of a system drastically. By decreasing the bandwidth and moving to non-UWB radio signals the specular components (including the line of sight (LOS)) are no longer separated from other multipath components which are denoted as dense or diffuse multipath (DM). This DM leads to multipath effects such as amplitude fading and pulse distortion. For narrowband signals only amplitude fading occurs since the complete DM interferes with the LOS component, while for the UWB case the LOS component is well-separated from the DM. The bottom of Fig. 1 illustrates these cases and shows the pulse distortion and amplitude fading at bandwidths in between these "extreme cases".

In [5] we derived the Cràmer Rao lower bound (CRLB) on ranging and positioning for a channel consisting of the LOS component and dense multipath. Within this paper

- we analyze the CRLB for the ranging error for different channel parameters,
- derive an approximation for the CRLB, and
- validate the model and CRLB using measurement data.

II. Signal Model

We consider L measurements obtained from signal transmissions between an agent at an unknown position $\mathbf{p}$ and anchors at known positions $\mathbf{a}_\ell$. A unit energy pulse $s(t)$ is transmitted leading to the received signal

$$r(t) = \alpha_\ell s(t-\tau_\ell) + (s * \nu_\ell)(t) + w(t), \tag{1}$$

where $\alpha_\ell = |\alpha_\ell| e^{-j(2\pi f_c \tau_\ell + \varphi_0)}$ describes the complex amplitude of the deterministic line-of-sight (LOS) component with delay $\tau_\ell = \frac{1}{c}\|\mathbf{p} - \mathbf{a}_\ell\|$, where c denotes the speed of light, f_c is the carrier frequency and φ_0 is a random phase offset. The second term denotes the dense multipath (DM) which is modeled as a zero-mean complex Gaussian random process. By assuming uncorrelated scattering in the delay domain, the auto-correlation of the DM process is given as

$$K_\nu^{(\ell)}(t,u) = \mathbb{E}_\nu\left\{\nu_\ell(t)\nu_\ell^*(u)\right\} = S_\nu^{(\ell)}(t-\tau_\ell)\delta(t-u), \tag{2}$$

where $S_\nu^{(\ell)}(t)$ is the power delay profile (PDP) of the DM process at position $\mathbf{p}$ as a function of the excess delay time. Quasi-stationarity in the spatial domain is assumed, meaning that the PDP does not change in the vicinity of the position $\mathbf{p}$. Finally, the third term in (1) models additive white Gaussian noise (AWGN).

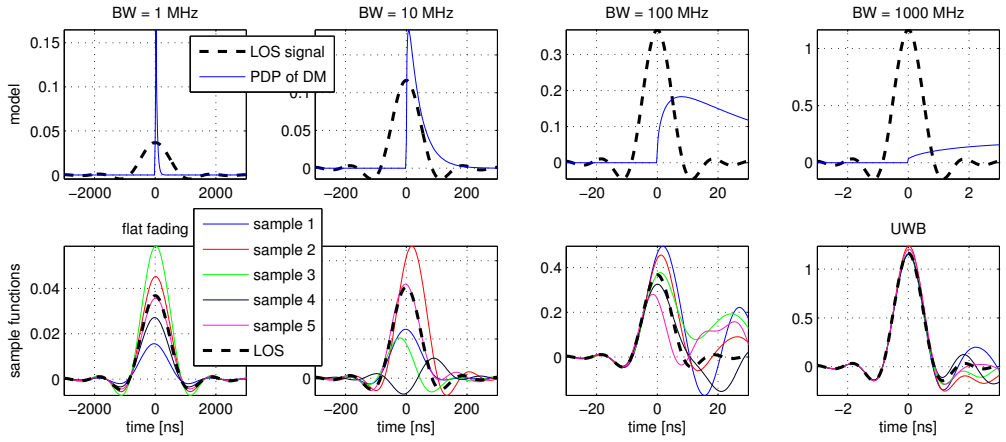

Fig. 1. Model and sample functions illustrating the problem under investigation over a wide range of BWs (neglecting AWGN).

The DM is modeled as double exponential function (cf. [6])

$$S_\nu^{(\ell)}(\tau) = \Omega_1 \frac{\gamma_{\text{dec}} + \gamma_{\text{rise}}}{\gamma_{\text{dec}}(\gamma_{\text{dec}} + \gamma_{\text{rise}}(1-\chi))}(1 - \chi e^{-\tau/\gamma_{\text{rise}}})e^{-\tau/\gamma_{\text{dec}}} \tag{3}$$

where Ω_1 is the total power of the DM, and γ_{rise}, γ_{dec}, and χ are shape parameters. The Rician K-factor for the LOS component is

$$K_{\text{LOS}} = \frac{|\alpha_\ell|^2}{\Omega_1}. \tag{4}$$

Fig. 1 illustrates the signal model and shows a few sample realizations of the received signal neglecting the AWGN. For high bandwidths (the UWB case) the DM process is clearly separated from the LOS component and neither fading nor distortion of the transmitted pulse occurs. By decreasing the bandwidth (BW) the interference between the transmitted pulse and the DM process increases and leads to fading and distortion of the received pulse. For low bandwidths the complete DM process interferes with the LOS component and only fading occurs. In the following the measurement index ℓ will be dropped.

III. Ranging Error Bound (REB)

In [5] we derived the REB, which is the square root of the inverse of the equivalent Fisher information (EFI) $\mathcal{R}(\tau) = \sqrt{\mathcal{I}_\tau^{-1}}$, the square root of the CRLB $\text{var}\{\hat{\tau}\} \geq \mathcal{I}_\tau^{-1}$ for the delay-estimation problem. This enables us to investigate the influence of the signal and environment model parameters onto the REB. Under the assumption that the AWGN and the DM are both Gaussian, the EFI for a single channel can be presented as

$$\mathcal{I}_\tau = 8\pi^2\beta^2\gamma\text{SINR}\sin^2(\phi) = 8\pi^2\beta^2\widetilde{\text{SINR}} \tag{5}$$

where $\beta^2 = \|\dot{\mathbf{s}}_\tau\|^2/(4\pi^2\|\mathbf{s}_\tau\|^2) = \int_f f^2|S(f)|^2\text{d}f$ is the effective (mean square) bandwidth of the (energy-normalized) transmit pulse $s(t) \overset{\mathcal{F}}{\longleftrightarrow} S(f)$, $\mathbf{s}_\tau$ is the sampled transmit pulse shifted to τ, $\dot{\mathbf{s}}_\tau$ is its derivative, SINR is the signal-to-interference-plus-noise ratio (SINR) of the LOS component, γ is the so-called whitening gain, and $\sin^2(\phi)$ incorporates the estimation of the nuisance parameter α. The product of β^2, SINR, γ, and $\sin^2(\phi)$ thus provides the amount of information transmitted in the LOS component when influenced by DM and AWGN. For the derivation of (5), the inverse of the covariance matrix of DM plus AWGN is needed as a whitening operator. The SINR, the whitening gain γ, and $\sin^2(\phi)$ are also combined in the effective SINR, $\widetilde{\text{SINR}}$ which can be expressed as [5]

$$\widetilde{\text{SINR}} = \frac{|\alpha|^2}{N_0}\|\mathbf{s}_\tau\|^2 T_s \frac{\|\dot{\mathbf{s}}_\tau\|_{\mathcal{H}}^2}{\|\dot{\mathbf{s}}_\tau\|^2}\sin^2(\phi), \tag{6}$$

where $T_\text{s} = 1/f_\text{s}$, f_s is the sampling frequency, $\|\cdot\|_{\mathcal{H}}^2$ denotes the weighted squared norm in a Hilbert space defined by the covariance $\mathbf{C}_\text{n}/\sigma_\text{n}^2$ (see Appendix A), and ϕ is the angle between $\mathbf{s}_\tau$ and its derivative $\dot{\mathbf{s}}_\tau$ in this Hilbert space. Appendix B introduces approximations for the previously defined parameters without the need to compute the inverse of the covariance matrix.

Fig. 2a illustrates the SINR, γ, $\sin^2(\phi)$, and $\widetilde{\text{SINR}}$ over a wide range of bandwidths for three different K_{LOS} factors (-10 dB, 0 dB, and 10 dB). For low BWs the SINR tends towards the Rician K_{LOS} factor of the channel model and for high bandwidth it reaches the signal to noise ratio (SNR). The SINR reflects the amplitude fading of the LOS component. The $\widetilde{\text{SINR}}$ follows the SINR at high bandwidth but reaches the SNR again at low bandwidth. The $\widetilde{\text{SINR}}$ reflects the pulse distortion of the deterministic LOS component. At high BW neither fading nor distortion occurs and both the SINR and $\widetilde{\text{SINR}}$ reach the SNR. By decreasing the BW, both amplitude fading and pulse distortion occur leading to decreased SINR and $\widetilde{\text{SINR}}$. At very low BW only amplitude fading occurs since the complete DM process interferes with the pulse (cf. Fig. 1). The parameter $\sin^2(\phi)$ which can be attributed to the cost of estimating the nuisance parameter α reduces the achievable whitening gain. The lower the K_{LOS} factor the higher the cost for estimating the nuisance parameter.

In Fig. 2b the shape parameter γ_{rise} of the double exponential PDP (3) is varied. If γ_{rise}, which describes the onset behaviour of the PDP, is set to zero the double exponential PDP reduces to an exponentially decaying PDP. Thus, for high BW some amplitude fading and pulse distortion occur as well and the $\widetilde{\text{SINR}}$ and SINR do not reach the SNR. The cost for

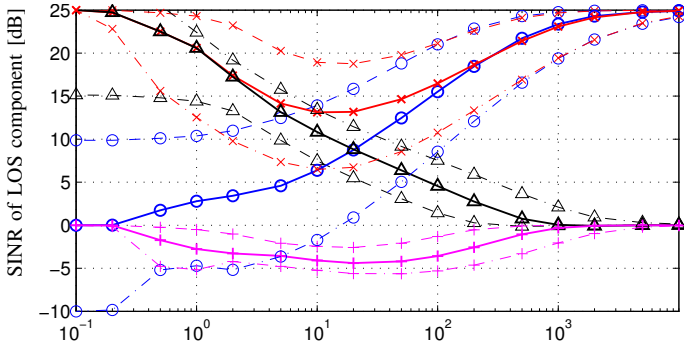

(a) K_{LOS}: dotted lines 10 dB, solid lines 0 dB, and chain dotted lines -10 dB)

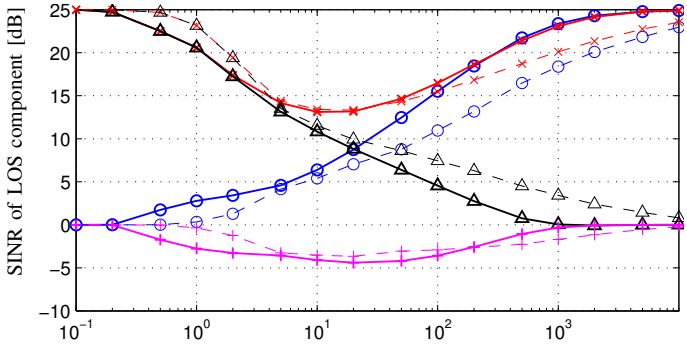

(b) γ_{rise}: solid lines 5 ns, and dotted lines 0 ns

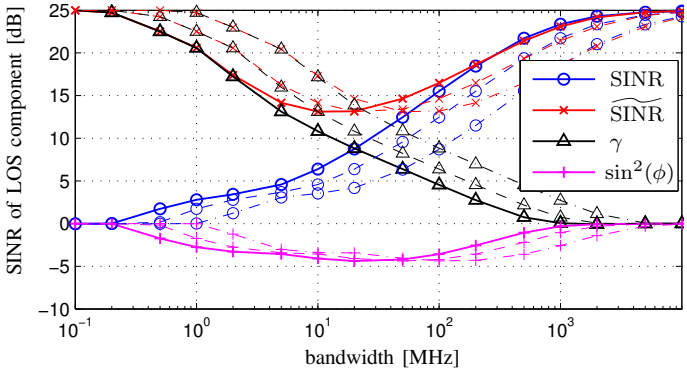

(c) γ_{rise} and γ_{dec}: solid lines 5 ns and 20 ns, dotted lines 2.5 ns and 10 ns, and chain dotted lines 1 ns and 4 ns respectively

Fig. 2. SINR, $\widetilde{\mathrm{SINR}}$, whitening gain γ, and $\sin^2(\phi)$ as a function of bandwidth and different channel parameters. If not stated otherwise: $\mathrm{E}_{\mathrm{LOS}}/N_0 = 25$ dB, $K_{\mathrm{LOS}} = 0$ dB, $\gamma_{\mathrm{dec}} = 20$ ns, $\gamma_{\mathrm{rise}} = 5$ ns.

estimating the nuisance parameter α is coupled with the pulse distortion. At low BW less pulse distortion occurs since the complete DM interferes with the LOS. In the region where the BW is approximately the inverse of the rms delay spread ($\tau_{\mathrm{rms}} = \{17.3, 16.1\}$ ns) the most pulse distortion occurs and the cost for estimating the nuisance parameter α is the highest. By varying both the shape parameters γ_{rise} and γ_{dec} by the same factor, it can be shown, that the root mean square (rms) delay spread of the PDP is changed by the same factor. Thus, in Fig. 2c the effect of different τ_{rms} is depicted. At low BW the $\widetilde{\mathrm{SINR}}$ is higher for smaller τ_{rms} since less pulse distortion occurs. At high BW, the lower τ_{rms} of the PDP, the higher the

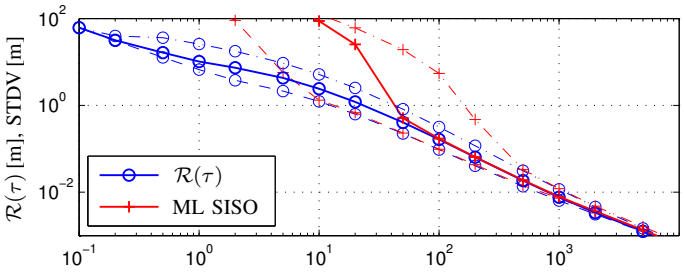

(a) REB and simulated range estimation error STDV for ML estimator

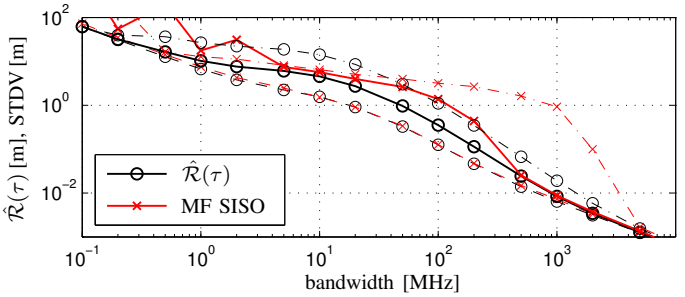

(b) Approx. REB and simulated range estimation error STDV for MF estimator

Fig. 3. REB, approximated REB, and simulated range estimation error STDV for ML and MF estimator for different K_{LOS} factors (solid lines 10 dB, dotted lines 0 dB, and chain dotted lines -10 dB). Other channel parameters: $\mathrm{E}_{\mathrm{LOS}}/N_0 = 25$ dB, $\gamma_{\mathrm{dec}} = 20$ ns, $\gamma_{\mathrm{rise}} = 5$ ns.

bandwidth needs to be for the same SINR and $\widetilde{\mathrm{SINR}}$.

In Fig. 3a the ranging error bound for three different K_{LOS}-factors (10 dB, 0 dB, -10 dB) is depicted. Two different gains can be seen in Fig. 3a: An accuracy gain can be identified by looking at the REB at the same bandwidth. The higher the Rician K-factor, the lower the REB for the same bandwidth. The second gain, a detection gain, is depicted by the standard deviation (STDV) of the ranging error of a maximum likelihood (ML) estimator which uses the inverse of the covariance matrix of the DM plus AWGN random process as whitening. For a small K_{LOS} factor the estimator starts to deviate from the REB at higher bandwidth. The detection of the LOS is coupled with the SINR which reflects the SNR after the whitening operation. Hence, for higher K_{LOS} factors, the ML estimator deviates from the REB at lower BW.

In Fig. 3b the STDV of the ranging error of a "naïve" matched filter (MF) estimator, which convolves the received signal with the transmitted pulse and searches for its maximum, is depicted along with the approximated values (Appendix B) for the REB. As long as the SINR is high enough, the MF estimator follows the approximation of the CRLB very well. Since the MF estimator projects the received signal onto the pulse, this estimator works in the signal space defined by the approximation for the inverse of the covariance matrix.

IV. Validation

To validate the theoretical results in the previous section we performed measurements with an M-sequence correlative channel sounder by *Ilmsens*, which provides measurements over approx. the proposed UWB frequency range from 3.5 - 10.5 GHz. Out of this band we selected the desired bandwidth

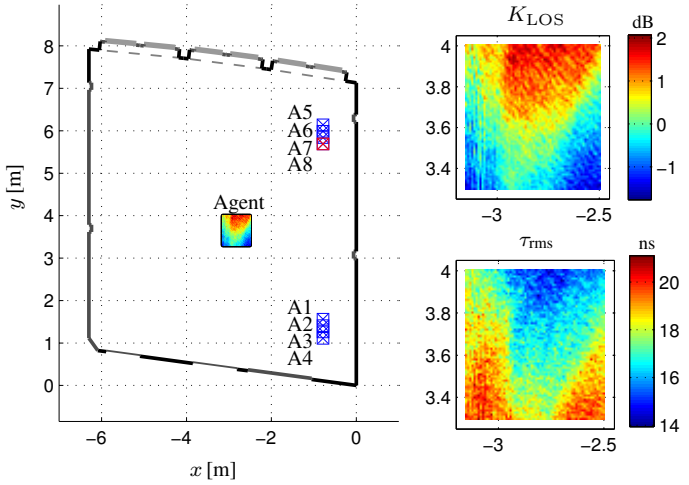

Fig. 4. Floorplan of the validation scenario. Positioning of the agent has been performed with a 2D positioning table with 1 cm-spacing. Measurements have been performed from the agent to eight anchors (A1 to A8) aligned as two linear arrays with 15 cm-spacing. The plot shows the instantaneous Rician K_{LOS} factors in dB and the instantaneous rms delay spreads τ_{rms} factors in ns as a color coded map with respect to Anchor 8.

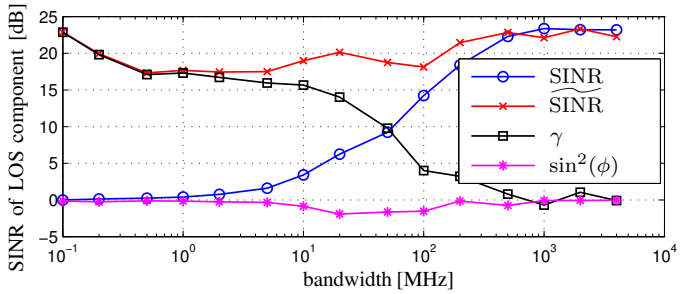

Fig. 5. SINR, $\widetilde{\mathrm{SINR}}$, and whitening gain γ as a function of bandwidth for Anchor 8. Channel Parameters: $K_{\mathrm{LOS}} = 0.31$ dB, $\tau_{\mathrm{rms}} = 17.53$ ns

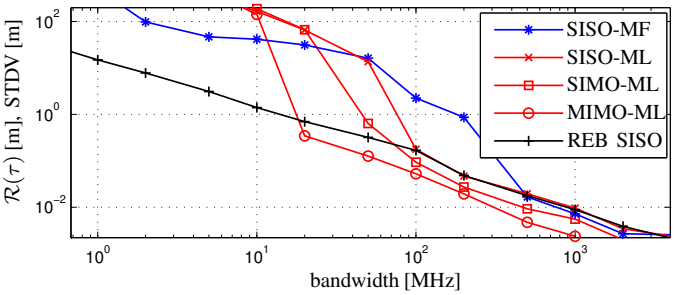

Fig. 6. Ranging Error Bound and range estimation standard deviations of different estimators. Channel Parameters: $K_{\mathrm{LOS}} = 0.31$ dB, $\tau_{\mathrm{rms}} = 17.53$ ns

by filtering with a root raised cosine pulse with a pulse duration ranging from 0.25 ns to 10 μs with roll-off factor 0.5. Fig. 4 shows the floorplan of the measurement scenario [7]. Measurements have been performed between an "agent" mounted on a 2D positioning table (70 cm times 65 cm spaced by 1 cm) to eight "anchors" arranged as two linear arrays spaced by 15 cm. Instantaneous Rician K_{LOS} factors are shown for each measurement from the agent to Anchor 8. The K_{LOS} factor is higher in regions closer to the anchor and is on average 0.31 dB. Instantaneous τ_{rms} are plotted in the lower right corner of Fig. 4 and is on average 17 ns.

The covariance matrix of the dense multipath, needed for the whitening operation, has been estimated from a 2 cm spaced 5x5 grid around the current measurement by subtracting the LOS component from the received signal. The complex amplitudes $\hat{\alpha}_\ell$ of the LOS component have been estimated at the highest possible BW (4 GHz) and are used at lower BWs to subtract the LOS component. AWGN has been added to the measurements to get a desired E_{LOS}/N_0 of 25 dB.

Fig. 5 shows the average values of the SINR, $\widetilde{\mathrm{SINR}}$, γ, and $\sin^2(\phi)$ for 42 measurements. The agent positions have been placed on the grid in such a way that each measurement is used only once to minimize correlation effects between different realizations. The SINR shows the same behavior as the theory. At low BW it tends towards the K_{LOS} factor and at high BW it is bound by the E_{LOS}/N_0. The whitening gain as well as the effective SINR show similar behaviors as the theory. The synthetic data in Fig. 2a and Fig. 3a with $K_{\mathrm{LOS}} = 0$ dB, $\gamma_{\mathrm{rise}} = 5$ ns, and $\gamma_{\mathrm{dec}} = 20$ ns lead to a $\tau_{\mathrm{rms}} = 17.3$ ns and thus compares best to the measured data.

In Fig. 6 the REB and the STDV of the estimation error are shown for two estimators. The MF estimator works at BWs higher than 500 MHz. At lower BWs a positive bias and outliers occur, which push the STDV of the MF estimator away from the theoretical bound. The ML estimator for a single-input, single-output (SISO) scenario starts to deviate from the REB at BWs below 100 MHz. The accuracy gain due to proper handling of the pulse distortion is clearly visible. The synthetic data presented in Fig. 3a for comparable channel parameters (K_{LOS}, τ_{rms}) deviates at about 50 MHz.

By using diversity at the anchor side, a single input, multiple output (SIMO) system can be realized. As shown in [5] additional uncorrelated measurements scale the effective SINR and the EFI linearly, thus the REB is scaled by the inverse of the square root of the number of receivers[1]. This factor of 1/2 is seen in Fig. 6 for the 1x4-SIMO ML estimator. By additionally combining agent measurements a multiple input, multiple output (MIMO) system is obtained. Again, four measurements, have been combined to evaluate the ranging performance of the overall 4x4-MIMO system. The accuracy gain is another factor of 1/2 for the STDV in comparison to the 1x4-SIMO system. Furthermore, a detection gain is achieved by combining measurements. The detection of the LOS, which is coupled with the SINR is enhanced and the STDV of the estimation error follows the REB down to lower BW. With the 4x4 MIMO system a ranging STDV of 30 cm can be obtained at a BW of 20 MHz.

V. Conclusions and Outlook

The ranging error bound has been analyzed for LOS signals in dense multipath (DM), evaluating the impact of signal parameters and environmental model parameters like the K_{LOS} and τ_{rms} factor. A higher K_{LOS} and higher τ_{rms} factor of the power delay profile are preferred. The theoretical findings have been validated with real measurement data. Strong early

[1]To obtain this diversity gain, the likelihood functions of individual measurements are added up, which corresponds to a non-coherent combining of measurements that require no phase coherence.

reflections still pose a challenge for the ranging algorithm, specifically the estimation of the covariance matrix, but it is seen that diversity gain can overcome the need for ultra-wideband signals to obtain high-accuracy positions in dense multipath channels.

Appendix A
Fisher Information for Delay Estimation

For a sampled received signal, the covariance matrix of AWGN and the DM is written as

$$\mathbf{C}_{\mathrm{n}} = \sigma_{\mathrm{n}}^2 \mathbf{I}_N + \mathbf{C}_{\mathrm{c}} = \sigma_{\mathrm{n}}^2 \mathbf{I}_N + \bar{\mathbf{S}}^{\mathrm{H}} \mathbf{S}_\nu \bar{\mathbf{S}} \tag{A.1}$$

where $\bar{\mathbf{S}} = [\mathbf{s}_0, \cdots, \mathbf{s}_{N-1}]^{\mathrm{T}} \in \mathbb{R}^{N\times N}$ is a signal matrix with $\mathbf{s}_i = [s((-i)T_{\mathrm{s}}), \ldots, s((N-1-i)T_{\mathrm{s}})]^{\mathrm{T}}$ [4]. The elements of the covariance matrix of DM are

$$[\bar{\mathbf{S}}^{\mathrm{H}} \mathbf{S}_\nu \bar{\mathbf{S}}]_{n,m} = \sum_{i=0}^{N-1} T_{\mathrm{s}} S_\nu(iT_{\mathrm{s}}) s((n-i)) s((m-i)). \tag{A.2}$$

The derivation of the EFI under non-stationary, non-white Gaussian noise, involves a whitening operation that is defined by the inverse of the covariance matrix. By utilizing an eigenvector decomposition for the covariance matrix, and introducing the Fourier-weighted inner product in a Hilbert space defined by [5]

$$\begin{aligned}\frac{\langle \mathbf{x}, \mathbf{y}\rangle_{\mathcal{H}}}{\sigma_{\mathrm{n}}^2} &= \mathbf{y}^{\mathbf{H}} \mathbf{C}_{\mathrm{n}}^{-1} \mathbf{x} = \mathbf{y}^{\mathbf{H}} \mathbf{U} (\mathbf{\Lambda} + \sigma_{\mathrm{n}}^2 \mathbf{I}_N)^{-1} \mathbf{U}^{\mathrm{H}} \mathbf{x} \\ &= \frac{1}{\sigma_{\mathrm{n}}^2} \sum_{i=0}^{N-1} \frac{\mathbf{y}^{\mathrm{H}} \mathbf{u}_i \mathbf{u}_i^{\mathrm{H}} \mathbf{x}}{\lambda_i/\sigma_{\mathrm{n}}^2 + 1}\end{aligned} \tag{A.3}$$

we can write the EFI as (cf. [5], [8])

$$\begin{aligned}\mathcal{I}_\tau =& 2\frac{|\alpha|^2}{\sigma_{\mathrm{n}}^2} \|\dot{\mathbf{s}}_\tau\|_{\mathcal{H}}^2 \sin^2(\phi) + \mathrm{tr}\left[\mathbf{C}_{\mathbf{n}}^{-1} \frac{\partial \mathbf{C}_{\mathbf{n}}}{\partial \tau} \mathbf{C}_{\mathbf{n}}^{-1} \frac{\partial \mathbf{C}_{\mathbf{n}}}{\partial \tau}\right] \\ =& 2\frac{|\alpha|^2}{\sigma_{\mathrm{n}}^2} \|\dot{\mathbf{s}}_\tau\|_{\mathcal{H}}^2 \left(1 - \frac{|\langle \dot{\mathbf{s}}_\tau, \mathbf{s}_\tau\rangle_{\mathcal{H}}|^2}{\|\dot{\mathbf{s}}_\tau\|_{\mathcal{H}}^2 \|\mathbf{s}_\tau\|_{\mathcal{H}}^2}\right) + \mathrm{tr}\left[\bullet\right]\end{aligned} \tag{A.4}$$

where the "tr $[\bullet]$-part" is for the impact of unknown parameters of the DM process, e.g. the unknown arrival time of the DM. We argue in [5] that this part can be neglected.

Writing the SINR as

$$\mathrm{SINR} = \frac{|\alpha|^2}{N_0} \|\mathbf{s}_\tau\|_{\mathcal{H}}^2 T_{\mathrm{s}} \tag{A.5}$$

the first part of (A.4 can be decomposed as in (5).

Appendix B
Approximated Inverse Covariance

Inspite of the different definitions, numeric evaluations are still needed to gain insight in the quantitative behavior of the introduced parameters. To address this issue, we introduce a decomposition of the covariance matrix into an orthonormal basis that allows the approximate numeric evaluation of the Hilbert norms. We decompose $\mathbf{C}_{\mathrm{n}}$ as

$$\mathbf{C}_{\mathrm{n}} = [\mathbf{u}_1, \mathbf{u}_2, \mathbf{U}_0] \begin{bmatrix} \begin{bmatrix} \eta & \rho \\ \rho^* & \eta' \end{bmatrix} & \mathbf{A} \\ \mathbf{A}^{\mathrm{H}} & \mathbf{\Lambda}_0 \end{bmatrix} \begin{bmatrix} \mathbf{u}_1^{\mathrm{H}} \\ \mathbf{u}_2^{\mathrm{H}} \\ \mathbf{U}_0^{\mathrm{H}} \end{bmatrix} \tag{B.1}$$

choosing orthonormal basis vectors $\mathbf{u}_1 = \mathbf{s}_\tau/\|\mathbf{s}_\tau\|$ and $\mathbf{u}_2 = \dot{\mathbf{s}}_\tau/\|\dot{\mathbf{s}}_\tau\|$ in directions of the LOS pulse and its derivative. The coefficients η, η', and ρ describe the statistics of these two components of noise vector $\mathbf{n}$. They are computed from $\mathbf{C}_{\mathrm{n}}$, e.g. $\rho = \mathbf{u}_1^{\mathrm{H}} \mathbf{C}_{\mathrm{n}} \mathbf{u}_2$. Matrix $\mathbf{A}$ expresses the correlation of the noise in these two directions and the other coordinate axes (in $\mathbf{U}_0$).

Using the Schur complement and assuming that the correlations $\mathbf{A}$ are negligible, the inverse of $\mathbf{C}_{\mathrm{n}}$ is written as

$$\begin{aligned}\mathbf{C}_{\mathrm{n}}^{-1} \approx& [\mathbf{u}_1, \mathbf{u}_2, \mathbf{U}_0] \\ &\times \begin{bmatrix} \begin{bmatrix} \eta' & -\rho \\ -\rho^* & \eta \end{bmatrix} \frac{1}{\eta\eta' - |\rho|^2} & \mathbf{X} \\ \mathbf{X}^{\mathrm{H}} & \mathbf{Z} \end{bmatrix} \begin{bmatrix} \mathbf{u}_1^{\mathrm{H}} \\ \mathbf{u}_2^{\mathrm{H}} \\ \mathbf{U}_0^{\mathrm{H}} \end{bmatrix}.\end{aligned} \tag{B.2}$$

Using this approximation, it is straightforward to compute approximated values for the parameters defined in Appendix A. From (A.4), we obtain

$$\mathcal{I}_\tau^{(\mathrm{I})} \approx 2 \underbrace{\frac{\|\dot{\mathbf{s}}_\tau\|^2}{\|\mathbf{s}_\tau\|^2}}_{4\pi^2\beta^2} \underbrace{\frac{\eta}{\eta'}}_{\approx\gamma} \underbrace{\frac{|\alpha|^2 \|\mathbf{s}_\tau\|^2 \eta'}{\eta\eta' - |\rho|^2}}_{\approx \mathrm{SINR}} \underbrace{\left(1 - \frac{|\rho|^2}{\eta\eta'}\right)}_{\approx \sin^2(\phi)}. \tag{B.3}$$

From this, the SINR (A.5) times $\sin^2(\phi)$ can be written as

$$\begin{aligned}\sin^2(\phi)\mathrm{SINR} \approx& |\alpha|^2 \|\mathbf{s}_\tau\|^2 \frac{1}{\eta} \\ =& |\alpha|^2 \frac{1}{N_0 + \sum_{i=0}^{N-1} [\boldsymbol{\varrho}_{\mathbf{s}}]_i^2 S_\nu(iT_{\mathrm{s}}) T_{\mathrm{s}}}\end{aligned}$$

where $\boldsymbol{\varrho}_{\mathbf{s}} = \bar{\mathbf{S}} \mathbf{s}_\tau T_{\mathrm{s}}$ is the autocorrelation sequence of waveform $s(t)$, whose norm is independent of T_{s}. This results shows that the interference power scales according to the inner product of the squared pulse ACF $\varrho^2(t)$ and the PDP $S_\nu(t)$. I.e., the greater the bandwidth, the better is the DM separated from the LOS component and the SINR converges towards the SNR. Using the results from (B.3), the effective SINR can be approximated by

$$\widetilde{\mathrm{SINR}} \approx |\alpha|^2 \|\mathbf{s}_\tau\|^2 \frac{1}{\eta'} \tag{B.4}$$

References

[1] Y. Shen, S. Mazuelas, and M. Z. Win, "Network Navigation: Theory and Interpretation," *Selected Areas in Communications, IEEE Journal on*, vol. 30, no. 9, pp. 1823–1834, Oct. 2012.

[2] H. Godrich, A. Haimovich, and R. Blum, "Target Localization Accuracy Gain in MIMO Radar-Based Systems," *IEEE Trans. Inf. Theory*, vol. 56, no. 6, pp. 2783 –2803, June 2010.

[3] D. Dardari, A. Conti, U. Ferner, A. Giorgetti, and M. Z. Win, "Ranging With Ultrawide Bandwidth Signals in Multipath Environments," *Proc. IEEE*, vol. 97, no. 2, pp. 404–426, Feb. 2009.

[4] E. Leitinger, P. Meissner, C. Ruedisser, G. Dumphart, and K. Witrisal, "Evaluation of Position-related Information in Multipath Components for Indoor Positioning," *IEEE J. Sel. Areas Commun.*, vol. 33, no. 11, pp. 2313 – 2328, Nov. 2015.

[5] K. Witrisal, E. Leitinger, S. Hinteregger, and P. Meissner, "Bandwidth Scaling and Diversity Gain for Ranging and Positioning in Dense Multipath Channels," *Wireless Communications Letters, IEEE*, 2016.

[6] J. Karedal, S. Wyne, P. Almers, F. Tufvesson, and A. F. Molisch, "A Measurement-Based Statistical Model for Industrial Ultra-Wideband Channels," *IEEE Transactions on Wireless Communications*, 2007.

[7] P. Meissner, "Multipath-Assisted Indoor Positioning," Ph.D. dissertation, Graz University of Technology, 2014.

[8] S. Kay, *Fundamentals of Statistical Signal Processing: Estimation Theory*. Prentice Hall Signal Processing Series, 1993.